Radiative and Conductive Heat Transfer in a Quiescent Gas-Solid Bed of Particles: Theory and Experiment

F. B. HILL and R. H. WILHELM

Princeton University, Princeton, New Jersey

This paper concerns a study of radiation as a contributing mechanism in the transfer of heat between discrete solid particles. A theory for transfer in such systems is generalized to include planar-, spherical-, and cylindrical-bed geometries; because of the particulate nature of the system the generalization is given in terms of finite-difference equations. Transfer experiments were performed in a quiescent cylindrical bed with an axial heat source and a cylindrical containing-wall sink. Heat fluxes and radial-temperature profiles were measured. As the experiments were arranged, only modest temperature gradients were established between source and sink, but the ambient sink temperature was taken in steps from 100° to 1,000°C. For a bed of 3.8-mm.-diameter alumina spheres the ratio of heat transferred by radiation to that transferred by conduction was estimated to increase with average bed temperature from the order of 0.1 at 100°C., to 1.2 at 1,000°C. The effects of temperature on bed reflectivity and transmissivity and on apparent boundary-temperature discontinuities are discussed.

Experimental indication of the relative importance of radiative and conductive heat transfer in quiescent gas-solid particle beds may be sought in measurements of the temperature dependence of the conductivity of such systems. On the assumption that the contribution of conduction is relatively temperature insensitive and that the radiation contribution depends strongly on temperature, an increase in conductivity with temperature will be largely an indication of an increase in the radiation contribution.

Few data at temperatures significant for radiation are available for interpretation. Many measurements have been made between room temperature and 100°C., where conductive heat transfer predominates. Since Waddams (*26*) summarized work in this temperature range prior to 1944, two additional sets of data (*19*, *27*) have appeared. Relatively fewer measurements have been made at temperatures above 100°C. Pirani and von Wangenheim (*17*) studied beds of various solids and particle sizes in air over a range of mean bed temperatures of from 460° to 800°C. Lucks, Linebrink, and Johnson (*12*) report conductivities of beds of foundry sands in air for three particle-size ranges from 260° to 1,230°C. Campbell and Huntington (*2*) have investigated evacuated beds of a number of industrially important particles and particle sizes at temperatures up to 360°C. The conductivities of beds of several solids and gases have been measured by Pollack (*18*) over a range of pressures (10 μ Hg to atmospheric pressure) and temperatures (room temperature to 340°C.). No evidence of convective heat transfer has been found for particles less than 0.5 cm. in diameter.

However with the exception of Pollack's work these measurements (as well as those below 100°C.) have been of over-all conductivities, which include wall effects and which are significantly smaller in value than local bed conductivities measured far from container walls, and the radiation contribution can best be found in practice from local conductivities. In addition, large temperature gradients, which tend to mask the effect of temperature level and to promote the interaction of radiation and conduction, were frequently employed in these measurements.

The interpretation of conductivity data usually involves the assumption that the conductivity of a bed of particles is the sum of the radiation and conduction contributions. Held (*7*) has shown this to be true for sufficiently small temperature gradients. Of the formulas proposed for the conduction contribution (*10*, *20*, *22*, *25*), the semitheoretical correlation of Schumann and Voss has been tested the most extensively. Wilhelm, Johnson, Wynkoop, and Collier (*28*) have derived a correction which enables prediction of 95% of a large body of data on over-all conductivities, obtained below 100°C., to within 8.5%. All expressions derived for the radiation contribution (*1*, *4*, *15*, *16*, *20*, *25*), expressed as a conductivity, have in common a dependence on cube of absolute temperature and on radiation-path length. None allows for the effects of all three processes, absorption, reflection, and transmission. All processes are considered by Hamaker (*6*) and by Held (*7*) in their treatments of the general problem of simultaneous radiative and conductive transfer. Also these authors have shown that near a container wall departure from the classical Fourier distribution exists and that the departure is due specifically to interaction of conduction and radiation.

In the present work Hamaker's theory, which was formulated for planar geometry in terms of continuous functions, is generalized to include cylindrical and spherical geometries. The generalization is given in terms of the calculus of finite differences, a form appropriate for systems composed of discrete particles. The

F. B. Hill is at Brookhaven National Laboratory, Upton, New York.

theory is compared with results of an experiment in which over-all and local conductivities were measured with small temperature gradients used at various levels between 100 and 1,000°C. Details beyond those presented here may be found in the study (*8*) upon which this paper is based.

THEORY

The radiation model presented here considers a bed of particles to be represented by a number of parallel surfaces with arbitrary spacing between successive surfaces, which, as interest may require, may be parallel planes of infinite extent, concentric cylinders of infinite length, or concentric spheres. Heat is assumed to flow in a direction perpendicular to the surfaces.

A set of such surfaces is considered, with index 1 through N. The medium contained between successive surfaces, representing the gas phase, is a perfect transmitter. Each surface is considered gray and is partially transparent, having a transmissivity τ, absorptivity α, and reflectivity ρ, with $\alpha + \rho + \tau = 1$. The fraction τ may be thought of as the effective fraction of open or free area through which radiant energy may be transmitted without absorption or reflection. The sum $\alpha + \rho$ may be thought of as representing the effective fraction of the area occupied by the packing. This fraction of the area is opaque to radiation. It emits, absorbs, and reflects radiant energy diffusely as a gray surface; that is, the absorptivity and reflectivity are constant and refer to total radiation.

The surfaces are bounded internally and externally by opaque isothermal surfaces, with indices zero and $N + 1$, and at the absolute temperatures T_0 and T_{N+1}, respectively, $T_0 > T_{N+1}$. The absorptivity and reflectivity of the inner bounding wall are α_0 and ρ_0, respectively, and those of the outer bounding wall are α_{N+1} and ρ_{N+1}, respectively. All surfaces, both opaque and partially transparent, are assumed to emit and reflect diffusely.

For this model the problem of interest is to calculate the temperature distribution in the partially transparent surfaces and the steady unidirectional heat transfer rate through the surfaces. From these results a quantity of interest in interpretation of data, the radiation conductivity of the model, may be derived. In the following paragraphs the mathematical formulation of the problem is presented, and the results of its solution are stated. Details of the solution are given in reference *8*.

The derivation is carried out in terms of concentric cylinders of infinite length or concentric spheres. Equations are derived by making energy balances based on a reference area of a given cylindrical or spherical surface. For concentric cylinders the areas referred to are areas per unit axial length; for spheres the areas are areas per sphere. Expressions appropriate for parallel planes of infinite extent may be obtained from the equations derived by assuming all the areas therein to be equal.

In the formulation of the problem, first all the surfaces are considered to be nonreflecting and, of the radiant energy which leaves a given convex or concave surface and which is diffusely distributed with respect to the given surface, the fraction which is incident on all other surfaces which the given surface can "see" is determined. The word *see* is used here in the sense that one surface includes another in its field of vision apart from the "dimming" of that vision by intervening partially transparent surfaces. The convex side of the ith surface is denoted by i^+ and the concave side by i^-.

The distribution of the radiant energy leaving a surface i^+, diffusely distributed with respect to i^+, over all surfaces which i^+ can see will be considered. In the absence of partially transparent surfaces between i and a surface m, $m > i$, all the energy must be incident on m^-, since i^+ cannot see itself and moreover can see only m^-, $m > i$. Thus in Figure 1 the field of vision of surface i^+, the convex side of surface i, includes only the concave side of surface m, that is m^-, where m has a radius greater than i, that is $m > i$. An observer located at the point P looking out from i^+ could see only those portions of m^- included between the lines PA and PB, as indicated by the arrows, and he could not see any portion of i^+. The effect of the presence of a partially transparent surface with transmissivity τ between i and m is to reduce the energy incident on m^- by the factor τ. Since there are $m - i - 1$ surfaces between i and m, the fraction of the energy incident on m^- is τ^{m-i-1}.

While a convex surface i^+ can see only one class of surfaces, a concave surface i^- can see three such classes. These classes are m^+, $m < i$; m^-, $m \leq i$; and m^-, $m > i$. Thus in Figure 2 the field of vision of the concave surface 3^- in the arbitrarily spaced concentric surfaces 0 to 7 is shown. Surface 0 is opaque, and all others are partially transparent. An observer located at the point P looking out from 3^- could see the three classes of surfaces referred to above and enumerated for this specific case as follows. Included in the class m^+, $m > i$ are 0^+, 1^+, and 2^+. The observer could see those portions of these surfaces which face the point P and which are included in the angles APA', BPB', and CPC', respectively. Included in the class m^-, $m \leq i$, are 1^-, 2^-, and 3^-. The observer could see those portions of 1^- included in the angles APB and $A'PB'$, those portions of 2^- included in the angles APC and $A'PC'$, and those portions of 3^- included in the angles APD and $A'PD'$. Finally included in the class m^-, $m > i$, are 4^-, 5^-, 6^-, and 7^-, of which the observer could see those portions included in the angles APD and $A'PD'$.

One may consider first the distribution of the radiant energy leaving i^-, diffusely distributed with respect to i^-, over the surfaces m^+, $m < i$. In the absence of partially transparent surfaces between i and m the fraction of the energy which is incident on m^+ has been shown to be S_m/S_i (*3, 21*). Since there are $i - m - 1$ partially transparent surfaces between i and m, the fraction of the energy incident on m^+ is $\tau^{i-m-1}(S_m/S_i)$.

With reference to the class m^-, $m \leq i$, Figure 3 will be considered, in which the surfaces i^- and m^- are indicated. Following the arguments of the preceding paragraph the fraction $\tau^{i-m}(S_{m-1}/S_i)$ of the energy leaving i^- is incident on $(m - 1)^+$, and since the fraction $\tau^{i-m}(S_m/S_i)$ is transmitted through m, then the fraction incident on m^-, $m \leq i$, is $\tau^{i-m}[(S_m - S_{m-1})/S_i]$. This fraction reaches m^- through the angles APB and $A'PB'$. It is apparent from what has been said above and from the figure that the fraction $\tau^{i-m+2}[S_{m-1} - S_{m-2})/S_i]$ of the energy leaving i^- is incident on m^- through the angles BPC and $B'PC'$, and so on for the other angles indicated. Summing the contributions for all such paths one finds that the total fraction of the energy incident on m^-, $m \leq i$, is

$$\tau^{i-m}\left[\frac{S_m - S_{m-1}}{S_i} + \tau^2\,\frac{S_{m-1} - S_{m-2}}{S_i} + \cdots + \tau^{2(m-1)}\,\frac{S_1 - S_0}{S_i}\right] = \tau^{i-m}\sum_{k=1}^{m}\tau^{2(m-k)}\,\frac{S_k - S_{k-1}}{S_i}$$

From this expression it is evident that the fraction of the energy leaving i^-, diffusely distributed with respect to i^-, which is again incident on i^-, is $\sum_{k=1}^{i}\tau^{2(i-k)}[(S_k - S_{k-1})/S_i]$.

Of any radiant energy incident on a concave surface the fraction τ is transmitted through the surface, and the transmitted energy then leaves a convex surface. As was previously shown, the fraction τ^{m-i-1} of the radiation leaving i^+ is incident on the convex surface m^-, $m > i$. Hence any radiation incident on a surface, i^-, is diminished by the factor τ^{m-i} on reaching the surface m^-, $m > i$. Therefore for the third class of surfaces, m^-, $m > i$, since the fraction $\sum_{k=1}^{i}\tau^{2(i-k)}[(S_k - S_{k-1})/S_i]$ of the radiation leaving i^- has been shown to be again incident on i^-, the fraction $\tau^{m-i}\sum_{k=1}^{i}\tau^{2(i-k)}[(S_k - S_{k-1})/S_i]$ is incident on m^-, $m > i$.

The results of the foregoing discussion are summarized in Table 1.

The surfaces of the model may reflect as well as absorb and transmit. The effect of reflection is to increase the amount of radiation leaving a concave

TABLE 1. DISTRIBUTION OF RADIANT ENERGY IN NONREFLECTING PARTIALLY TRANSPARENT SURFACES

Radiant energy is diffusely distributed with respect to source. Geometry is that of arbitrarily spaced concentric cylinders or spheres. Innermost surface is opaque.

Fraction of source energy incident on receiver

Source	Receiver m^+, $m < i$	m^-, $m \leq i$	m^-, $m > i$
i^+	0	0	τ^{m-i-1}
i^-	$\tau^{i-m-1}\dfrac{S_m}{S_i}$	$\tau^{i-m}\displaystyle\sum_{k=1}^{m}\tau^{2(m-k)}\dfrac{S_k - S_{k-1}}{S_i}$	$\tau^{m-i}\displaystyle\sum_{k=1}^{i}\tau^{2(i-k)}\dfrac{S_k - S_{k-1}}{S_i}$

surface above that leaving a nonreflecting concave surface. Since a concave surface can see itself, a certain fraction of the diffuse radiation leaving such a surface will again be incident on the surface. If the surface is nonreflecting, part of this fraction will be transmitted through the surface and the remainder will be absorbed by the surface. However for a reflecting surface with the same transmissivity some reflection (in effect reemission) will occur at the expense of absorption. Such a result is applicable only for concave surfaces, for, since convex surfaces cannot see themselves, "internal" reflections cannot occur at these surfaces.

It has been seen that, of the diffusely distributed radiant energy leaving i^-, in the absence of reflection the fraction $\tau^{i-m-1}(S_m/S_i)$ is incident on m^+, $m < i$, and the fraction

$$\sum_{k=1}^{i}\tau^{2(i-k)}\left[\frac{(S_k - S_{k-1})}{S_i}\right]$$

is incident on i^-. When, in the presence of reflection, this latter fraction of the energy is reflected by i^-, it becomes diffusely distributed with respect to i^-. In effect the fraction

$$\rho_i\sum_{k=1}^{i}\tau^{2(i-k)}\left[\frac{(S_k - S_{k-1})}{S_i}\right]$$

of the energy is reemitted by i^-, and consequently the additional fraction

$$\tau^{i-m-1}\frac{S_m}{S_i}\rho_i\cdot\sum_{k=1}^{i}\tau^{2(i-k)}\left[\frac{(S_k - S_{k-1})}{S_i}\right]$$

is incident on m^+, $m < i$, and

$$\sum_{k=1}^{i}\tau^{2(i-k)}\left[\frac{(S_k - S_{k-1})}{S_i}\right]\rho_i\cdot\sum_{k=1}^{i}\tau^{2(i-k)}\left[\frac{(S_k - S_{k-1})}{S_i}\right]$$

is again incident on i^-. This process is repeated ad infinitum with the result that the total fraction of the diffusely distributed energy leaving i^- which is incident on m^+, $m < i$, is

$$\tau^{i-m-1}\frac{S_m}{S_i}\cdot\left[1 + \rho_i\sum_{k=1}^{i}\tau^{2(i-k)}\frac{S_k - S_{k-1}}{S_i} + \left(\rho_i\sum_{k=1}^{i}\tau^{2(i-k)}\frac{S_k - S_{k-1}}{S_i}\right)^2 + \cdots\right] = \frac{\tau^{i-m-1}\dfrac{S_m}{S_i}}{1 - \rho_i\displaystyle\sum_{k=1}^{i}\tau^{2(i-k)}\frac{S_k - S_{k-1}}{S_i}}$$

Similar arguments applied to the other two classes of surfaces which i^- can see demonstrate that consideration of reflection leads to the same modification of all expressions in Table 1 related to a source i^-, namely multiplication of these expressions by the factor

$$\frac{1}{1 - \rho_i\displaystyle\sum_{k=1}^{i}\tau^{2(i-k)}\frac{S_k - S_{k-1}}{S_i}}$$

The results of the arguments regarding reflecting surfaces are summarized in Table 2.

For the reference area S_m of the surface m the sum of the emitted and reflected radiant energy per unit time of the surface m^+ may be defined as the radiance energy I_m, and the same quantity for the surface m^-, not including contributions from internal reflections at m^-, may be defined as the radiance energy J_m. By virtue of the specification of diffuse emission and reflection of the surfaces the radiance energies I_m and J_m are diffusely distributed with respect to m^+ and m^-,

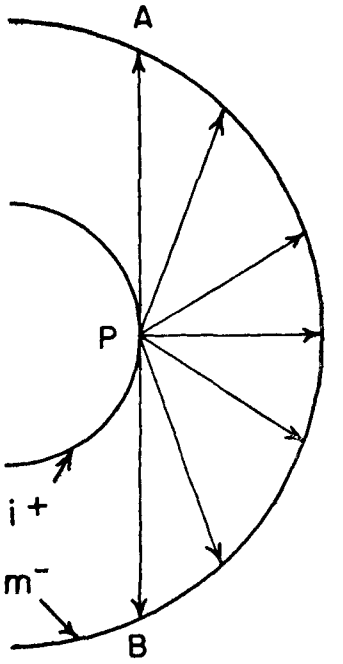

Fig. 1. Field of vision of a convex surface.

respectively. With the foregoing definitions and the aid of Table 2, the following expressions for I_m and J_m may be written:

$$I_m = \alpha_m W_m + \rho_m\sum_{i=m+1}^{N+1}\frac{\tau^{i-m-1}\dfrac{S_m}{S_i}}{1 - \rho_i\displaystyle\sum_{k=1}^{i}\tau^{2(i-k)}\frac{S_k - S_{k-1}}{S_i}}J_i, \qquad m = 0, 1, \cdots, N \qquad (1)$$

$$J_m = \alpha_m W_m + \rho_m\left[\sum_{i=0}^{m-1}\tau^{m-i-1}I_i + \sum_{i=1}^{m-1}\frac{\tau^{m-i}\displaystyle\sum_{k=1}^{i}\tau^{2(i-k)}\frac{S_k - S_{k-1}}{S_i}}{1 - \rho_i\displaystyle\sum_{k=1}^{i}\tau^{2(i-k)}\frac{S_k - S_{k-1}}{S_i}}J_i + \sum_{i=m+1}^{N+1}\frac{\tau^{i-m}\displaystyle\sum_{k=1}^{m}\tau^{2(m-k)}\frac{S_k - S_{k-1}}{S_i}}{1 - \rho_i\displaystyle\sum_{k=1}^{i}\tau^{2(i-k)}\frac{S_k - S_{k-1}}{S_i}}J_i\right], \quad m = 1, 2, \cdots, N+1 \qquad (2)$$

The first term on the right-hand side of each equation represents the radiant emission of the surface m given by the Stefan-Boltzmann law:

$$\alpha_m W_m = \alpha_m\sigma T_m^4 S_m$$

The remaining term or terms on the right-hand side of the equations represent the reflected radiation. Thus in Equation (1) from each of the surfaces i^-, $m < i \leq N + 1$, the radiance energy

$$\frac{\tau^{i-m-1}\dfrac{S_m}{S_i}}{1 - \rho_i\displaystyle\sum_{k=1}^{i}\tau^{2(i-k)}\frac{S_k - S_{k-1}}{S_i}}J_i$$

is incident on m^+. Hence the reflected energy contributing to I_m is

$$Q = \sum_{i=0}^{m} \tau^{m-i} I_i + \sum_{i=1}^{m} \frac{\tau^{m-i+1} \sum_{k=1}^{i} \tau^{2(i-k)} \frac{S_k - S_{k-1}}{S_i}}{1 - \rho_i \sum_{k=1}^{i} \tau^{2(i-k)} \frac{S_k - S_{k-1}}{S_i}} J_i$$

$$+ \sum_{i=m+1}^{N+1} \frac{\tau^{i-m+1} \sum_{k=1}^{m} \tau^{2(m-k)} \frac{S_k - S_{k-1}}{S_i}}{1 - \rho_i \sum_{k=1}^{i} \tau^{2(i-k)} \frac{S_k - S_{k-1}}{S_i}} J_i$$

$$- \sum_{i=m+1}^{N+1} \frac{\tau^{i-m-1} \frac{S_m}{S_i}}{1 - \rho_i \sum_{k=1}^{i} \tau^{2(i-k)} \frac{S_k - S_{k-1}}{S_i}} J_i, \qquad m = 0, 1, \cdots, N \tag{3}$$

$$\rho_m \sum_{i=m+1}^{N+1} \frac{\tau^{i-m-1} \frac{S_m}{S_i}}{1 - \rho_i \sum_{k=1}^{i} \tau^{2(i-k)} \frac{S_k - S_{k-1}}{S_i}} J_i$$

In Equation (2) the energy is reflected by the receiver m^-, for which the sources are for the terms in order, i^+, $m > i$; i^-, $m > i$; and i^-, $m < i$.

The second summation in Equation (2) is zero for $m = 1$, and the third summation is zero for $m = N + 1$. Also

$$\alpha_m = \alpha_0, \quad \rho_m = \rho_0 \quad \text{for} \quad m = 0$$

$$\alpha_m = \alpha, \quad \rho_m = \rho \quad \text{for} \quad m = 1, 2, \cdots, N$$

$$\alpha_m = \alpha_{N+1}, \quad \rho_m = \rho_{N+1} \quad \text{for} \quad m = N + 1$$

The steady radial rate of heat transfer per reference area is equal to the net radiance energy transfer in the direction of decreasing temperature; that is it is the radiance energy passing through the surface m^+ in the direction of increasing m minus the radiance energy incident on m^+ from the opposite direction. Again with the help of Table 2

$$I_m' = \sum_{i=0}^{m} \tau^{m-i} I_i \tag{4}$$

$$J_m' = \sum_{i=m}^{N+1} \frac{\tau^{i-m} \frac{S_{m-1}}{S_i}}{1 - \rho_i \sum_{k=1}^{i} \tau^{2(i-k)} \frac{S_k - S_{k-1}}{S_i}} J_i \tag{5}$$

Reference 8 gives the complete solution as well as a suggested method for numerical solution in the presence of conduction.

In the absence of conduction the temperature distribution, radial radiant heat transfer rate, and local radiation conductivity are found to be given by

$$\frac{T_0^4 - T_m'^4}{T_0^4 - T_{N+1}^4} = \frac{\frac{1}{\alpha_0 S_0} + \frac{1 + \rho - \tau}{1 - \rho + \tau} \sum_{i=1}^{m} \frac{1}{S_i} - \frac{1}{1 - \rho + \tau} \frac{1}{S_m}}{\frac{1}{\alpha_0 S_0} + \frac{1 + \rho - \tau}{1 - \rho + \tau} \sum_{i=1}^{N} \frac{1}{S_i} + \frac{\rho_{N+1}}{\alpha_{N+1} S_{N+1}}} \tag{6}$$

$$Q = \frac{\sigma(T_0^4 - T_{N+1}^4)}{\frac{1}{\alpha_0 S_0} + \frac{1 + \rho - \tau}{1 - \rho + \tau} \sum_{i=1}^{N} \frac{1}{S_i} + \frac{\rho_{N+1}}{\alpha_{N+1} S_{N+1}}} \tag{7}$$

$$k_{r_m} = \frac{4\sigma \Delta r_m T_m'^3}{\frac{1}{1 - \rho + \tau} \frac{S_m'}{S_m} + \frac{\rho - \tau}{1 - \rho + \tau} \frac{S_m'}{S_{m+1}}} \tag{8}$$

The positive terms on the right-hand side represent in order the sources i^+, $m > i$; i^-, $m \geq i$; and i^-, $m < i$. The receiver is m^-. Following incidence on m^-, the energy from these sources is transmitted through m and consequently in computing their contribution to Q the corresponding terms in Table 2 are each multiplied by τ. The last term in Equation (3) represents the contributions of the sources i^-, $m < i$, to the energy incident on the receiver m^+. If conduction and radiation are assumed to occur simultaneously, the term

$$\left[\frac{(k_{c_m} S_m')}{(r_{m+1} - r_m)}\right](T_{m+1} - T_m) - \left[\frac{(k_{c_{m-1}} S_{m-1}')}{(r_m - r_{m-1})}\right](T_m - T_{m-1})$$

is added to the right-hand side of Equation (3). The quantity S_m' is an appropriate average area for unidirectional conduction through the region bounded by the surfaces m amd $m + 1$.

Equations (1) to (3) constitute the mathematical formulation of the problem. The similarity of these equations to those of Hamaker (6) is discussed elsewhere (8).

In the absence of conduction the solution is straight forward after the following change of variables has been made:

Equation (8) is valid for small temperature gradients.

The temperature dependent parts of the local radiation conductivity include not only the factor T_m^3 but also those terms containing the radiation constants α_0, ρ_0, ρ, τ, α_{N+1}, and ρ_{N+1}. These constants are assumed not to vary with temperature over small temperature ranges. However they may vary appreciably with large changes in temperature level, the reflectivity of nonmetals increasing with temperature and that of metals decreasing with increasing temperature. Ratios of areas in the bed are assumed not to vary

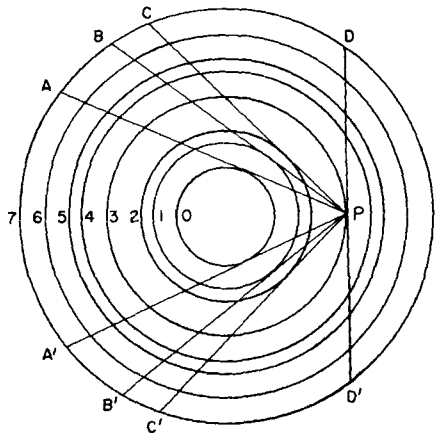

Fig. 2. Field of vision of a concave surface.

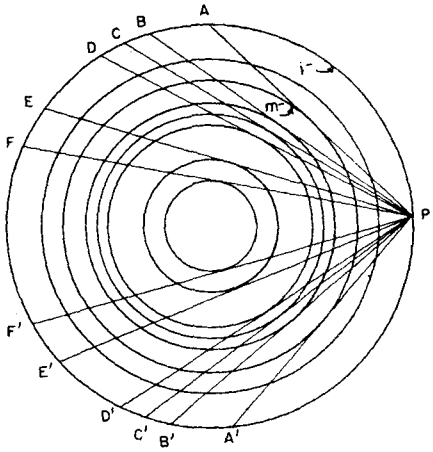

Fig. 3. Field of vision of i^- for m^-, $m \leq i$.

significantly with temperature. The local radiation conductivity is independent of wall properties but varies with position.

RELATION OF α, ρ, AND τ TO RADIATION CHARACTERISTICS OF PARTICLES OF BED

Some estimate of the relation of α, ρ, and τ, the effective radiation constants of the bed, to R, the reflectivity, and $A = 1 - R$, the absorptivity, of the surface of the particles of which the bed is composed, may be obtained by reference to Figure 4. In Figure 4 a small bundle of rays of radiant energy originating at particle 1 in a given layer is shown being distributed as a result of encountering particle 2 in another layer. Only a small bundle need be considered, since all such bundles, regardless of orientation with respect to their source layer, are assumed to suffer reflection and transmission to the same extent, characterized by the constants ρ and τ, upon being incident on a receiver layer. Some rays, A and B, are incident on particle 2; others, such as C, miss particle 2. These rays may be counted as being scattered forward. If the fraction of the energy leaving particle 1 which is not incident on particle 2 is T, then the fraction of this energy incident on particle 2 is $1 - T$. Of this fraction the fraction p is scattered backward and the fraction $1 - p$ is scattered forward. Then α may be taken to be

$$\alpha = (1 - T)(1 - R) \qquad (9)$$

and ρ is then

$$\rho = p(1 - T)R \qquad (10)$$

The quantity τ is used to represent forward scattered radiation. It must, on the basis of this discussion, include radiation actually reflected in the forward direction and radiation which misses a particle altogether. Thus

$$\tau = T + (1 - p)(1 - T)R \qquad (11)$$

A quantity of experimental interest is

$$\rho - \tau = (2p - 1)(1 - T)R - T \qquad (12)$$

The constants p and T are cosine-law view factors averaged over all possible relative positions of a particle and its nearest neighbors. Calculation of these constants is difficult if not impossible; probably they may be best determined experimentally.

EXPERIMENTAL

The thermal conductivity of a quiescent air-solid particle bed was measured as a function of temperature level and temperature gradient in an apparatus with cylindrical geometry (Figure 5). The bed was placed in a type-310 stainless steel container (4.75-in. I.D. by 24.1-in. inside length) having a tubular Calrod heater along its axis. For a given steady rate of radial heat flow through the bed, the steady state temperature distribution within the bed and at bounding surfaces was measured by thermocouples. The container was placed within a furnace which was used to produce a given temperature level within the bed upon which relatively small temperature gradients were imposed by means of the inner tubular heater.

The Calrod heater was 0.32 in. in diameter. Coil spacing over its effective heating length was found to be uniform by means of X-ray photographs. When installed in the apparatus, the effective heating length, which was greater than the length of the bed container, was centrally located with respect to the apparatus mid-plane.

Temperature was measured by means of thirteen chromel-alumel and two Pt-Pt 10% Rh thermocouples. The platinum thermocouples were calibrated at seventeen points between 0 and 1,500°C. by the National Bureau of Standards. The calibration had an uncertainty at the calibration points of 0.2°C. for temperatures less than 1,100°C. The chromel-alumel couples were calibrated in place by reference to the platinum couples. The measuring junctions of five thermocouples were placed within the bed at different radial positions at the bed mid-plane. The remainder were spot welded to the Calrod heater or were inserted in holes in the wall of the stainless steel container at the mid-plane and at points 9 in. above and below the mid-plane. A special tool inserted into the container during assembly was used to measure the radial position of measuring junctions within the bed. Thermocouple emf was measured with a potentiometer. Reference junctions were immersed in an ice bath.

An electromechanical voltage regulator supplied a voltage regulated to within 1% to two variable voltage autotransformers, one for the furnace and one for the Calrod heater.

The power supplied to the heater was measured with a wattmeter and a voltmeter.

The particles used in the experiments were alumina spheres. The particles were approximately spherical and nonporous. The mean particle diameter, based on the measurement of the diameters of 100 particles, was 3.81 ± 0.04 mm. Particle density as determined by duplicate pycnometer measurements was 3.49 g./cc.

Measured temperature distributions were corrected for the so-called "background temperature distribution." This distribution is the one obtained at any given temperature level with no power applied to the inner heater and is due to differences in thermocouple emf–temperature relations as well as to a nonisothermal temperature distribution. Ideally all temperatures throughout the bed should be the same under these conditions. In practice temperature differences of as much as 5°C. were found at the apparatus midplane, although the differences were usually not more than about 1°C. On the assumption that the steady state temperature distributions with and without power applied to the inner heater are describable by linear equations, the difference between these two distributions was taken to be the distribution corresponding to the radial heat flow.

Calculations were made which showed that the temperature distribution at the mid-plane of the bed of finite length was identical to that of an infinitely long bed

TABLE 2. DISTRIBUTION OF RADIANT ENERGY IN REFLECTING PARTIALLY TRANSPARENT SURFACES

Radiant energy is diffusely distributed with respect to source. Geometry is that of arbitrarily spaced concentric cylinders or spheres. Innermost surface is opaque.

Fraction of source energy incident on receiver

Source	Receiver m^+, $m < i$	Receiver m^-, $m \leq i$	Receiver m^-, $m > i$
i^+	0	0	τ^{m-i-1}
i^-	$\dfrac{\tau^{i-m-1}\dfrac{S_m}{S_i}}{1 - \rho_i \sum_{k=1}^{i} \tau^{2(i-k)} \dfrac{S_k - S_{k-1}}{S_i}}$	$\dfrac{\tau^{i-m} \sum_{k=1}^{m} \tau^{2(m-k)} \dfrac{S_k - S_{k-1}}{S_i}}{1 - \rho_i \sum_{k=1}^{i} \tau^{2(i-k)} \dfrac{S_k - S_{k-1}}{S_i}}$	$\dfrac{\tau^{m-i} \sum_{k=1}^{i} \tau^{2(i-k)} \dfrac{S_k - S_{k-1}}{S_i}}{1 - \rho_i \sum_{k=1}^{i} \tau^{2(i-k)} \dfrac{S_k - S_{k-1}}{S_i}}$

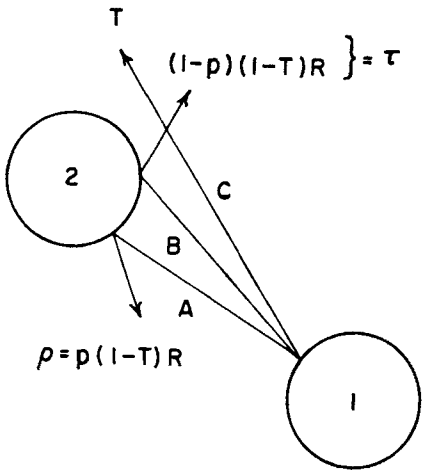

Fig. 4. Illustration of relation of ρ and τ to R and T.

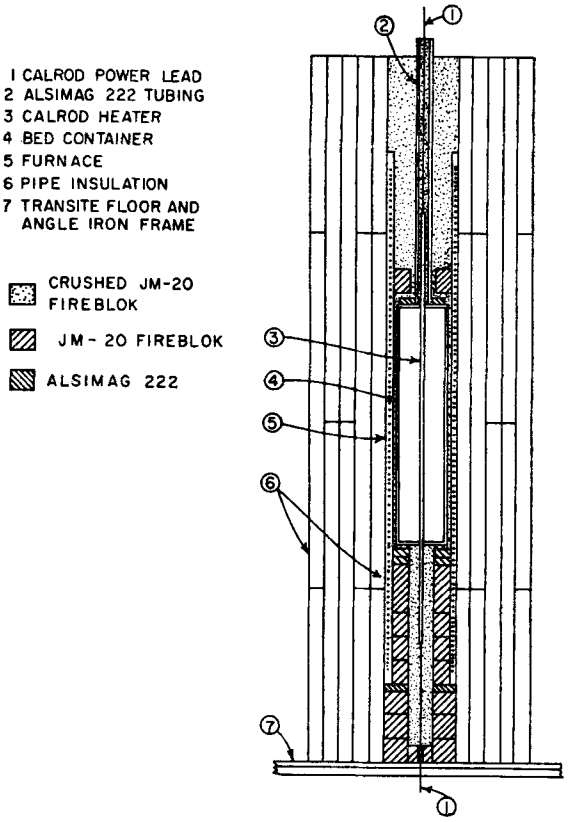

Fig. 5. Apparatus.

of the same diameter. Similar conclusions regarding this method were obtained by van Rinsum (*24*). Upon the application of a method presented by van Rinsum to the experimental data, it was found that, within the accuracy of the experiment, axial heat flow in the heater at the apparatus mid-plane was negiligible. Hence the heat-release rate and the temperature distribution at this position could be used in formulas appropriate for purely radial transfer. Experimental temperature distributions, corrected for background, were in good agreement with theoretical distributions, the agreement being better at high temperatures and small temperature gradients.

Course of Experiments

For a series of experiments at a given nominal temperature level (corresponding to a fixed furnace voltage) the furnace and its contents were first brought to temperature with no power on the Calrod heater. A period of about 4 to 5 days was required to establish temperature equilibrium. On each of the last 2 or 3 days of this period all thermocouple voltages were measured at 30-min. intervals for a period of $4\frac{1}{2}$ hr., and so ten sets of values of these variables were obtained. The variation of thermocouple voltages within the data for a given day and the variation of these voltages between data for successive days were used as the criteria for the establishment of steady state temperature distributions. The background temperature distribution was obtained in this way.

Then without a change in the furnace voltage, power was applied to the Calrod heater. As in the determination of the background distribution, time (3 to 4 days) was required for the establishment of steady temperatures. Measurement of the power consumed by the heater was made along with the same measurements of thermocouple voltages made in the background experiment.

A further experiment at the same nominal temperature level was carried out by changing the Calrod power to a new value and repeating the foregoing procedure.

The time variation of the individual temperature differences obtained from the resulting data (temperature in bed relative to container wall temperature, corrected for background) was of the order of 0.1 to 0.2°/hr., and conductivities computed from the averaged data for two successive days differed on the average by about 2% in an unsystematic way.

For several temperatures and especially at the highest temperatures investigated, the influence of heater and furnace voltages on thermocouple emf was determined by turning off power to these components momentarily and noting the resulting change in emf. No effect was found at low temperatures, and at the highest temperature level differences of as much as 8 μv. were found, for which correction was made.

RESULTS

Data, shown in Table 3, were obtained from a single packing of the container with the alumina particles described above used in air at atmospheric pressure. Temperature distributions were measured at four nominal temperature levels—100°, 400°, 700°, 1,000°C. and at several heat fluxes at each temperature level except at 1,000°C. The temperature levels are referred to as *nominal*, since for each heat flux at a given level the power applied to the furnace was kept constant and each increase in heat flux caused an increase in temperature level in the apparatus. Just one heat flux was used at 1,000°C. because during the equilibration period for a second flux the heater burned out and no further experiments were performed. Experiments are numbered in Table 3 in the order in which they were performed, generally in the order of increasing temperature level to avoid the effects of compression of the bed by the container on cooling.

Heat transfer rates in Table 3 were obtained from mean values of Calrod power corrected for the power consumed by the wattmeter and voltmeter and for the power consumed by the Calrod circuit apart from the central heating section. Also the elongation of the heater with temperature was taken into account. As stated earlier, no correction for axial heat flow was required. The temperature differences in Table 3 are indicated in Figure 6. It may be noted that in experiment 3, ΔT_c was negative. No reasonable explanation for this fact has been found.

Figure 6 shows a typical radial distribution at the apparatus mid-plane. Temperatures are corrected for background and are referred to container wall temperature. The abscissa is the finite differences function appropriate for purely radial transfer. These distributions exhibited the features predicted by Hamaker (*6*) and Held (*7*), namely a

Fourier distribution far from boundaries and departures from it near boundaries.

The distance coordinate in Figure 6 was calculated in the following way. The average particle spacing was evaluated by means of a relation proposed by Smith (*23*) for a rhombohedral array of spherical particles:

$$(\Delta r)^3 = 0.74\, D_p^3/(1 - f), \quad (13)$$

in which D_p was 0.38 cm. and f was 0.38. The particle spacing or radial distance between centers of successive particle layers, Δr, was then 0.40 cm. If f is 0.6 adjacent to the boundaries, the distance from a boundary to the center line of the adjacent layer is 0.47 cm. by the same formula. To accommodate radially an integral number of particle layers, namely 13, in the container, the average particle spacing in the bed proper was arbitrarily reduced to 0.39 cm. From these quantities the radius of each layer or surface was calculated. For the calculation of conductivities it was assumed that the average of two successive such radii was the appropriate radius upon which to base the area for heat transfer. Because the particle spacing was not uniform but was different at the walls from that in the bed, the function $\sum_{i=1}^{m} (\Delta r_i/S_i')$ was used as the distance coordinate for radial transfer rather than $\sum_{i=1}^{m} (1/S_i')$. Since the location of thermocouples within the bed did not coincide with the assumed location of particle layers, the value of the summation for a given couple was determined from a plot of $\sum_{i=1}^{m} (\Delta r_i/S_i')$ vs. r.

Local and over-all conductivities and boundary heat transfer coefficients derived from the data are given in Table 4 with corresponding average temperatures. These data are plotted in Figures 7 and 8. Conductivities were calculated from

$$k = \frac{[\text{radial heat transfer rate, cal./(sec)(cm)}]\left[\sum_{i=1}^{14} \frac{\Delta r_i}{S_i'}\right]}{\Delta T} \quad (14)$$

where ΔT_b was used for k_b and ΔT_{ov} for k_{ov}. The summation $\sum_{i=1}^{14} (\Delta r_i/S_i')$ had the value 0.351. The abscissa in Figure 7 is the temperature corresponding to the mid-point of the temperature drop associated with each conductivity. Both conductivities increased approximately linearly with temperature at low temperatures and increased more rapidly when the temperature exceeded 600°C. The local conductivity was greater than the over-all conductivity by about 40% at all temperatures.

Apparent boundary-temperature discontinuities (Figure 6) are shown in Table 4 and Figure 8 as apparent heat transfer coefficients with the units calories per second per square centimeter of bounding surface per degree centigrade temperature discontinuity. The abscissa in Figure 8 is the temperature corresponding to the mid-point of the temperature drop associated with each coefficient. The scatter exhibited by the coefficients was expected, for the temperature differences measured at the container wall were small, and at the Calrod heater the temperature differences involved the subtraction of data from base metal couples from that from platinum couples. There was nevertheless evident a trend of increasing coefficient with increasing temperature at both boundaries.

The accuracy of the conductivities is estimated to range from 5 to 25%, the smaller value applying for experiments involving the largest heat fluxes. The average accuracy of the boundary coefficients is about 50%.

The groups of points corresponding to each nominal temperature level are identified in Figures 7 and 8.

TABLE 3. DATA

Experiment no.	Nominal temperature level, °C.	Radial heat transfer rate, cal./(sec.)(cm. of heater length)	Wall temperature, °C.	Temperature difference, corrected for background, °C. ΔT_{ov}	ΔT_c	ΔT_b	ΔT_w
1	100	0.0362	105	15.0	2.5	12.1	0.4
2	100	0.0082	90	3.8	1.1	2.6	0.1
3	100	0.0797	127	25.8	−0.5	25.5	0.8
4	100	0.1477	154	71.0	22.2	46.8	2.0
5	100	0.0794	126	29.6	3.8	25.1	0.7
6	400	0.0390	402	12.5	3.8	8.4	0.3
7	400	0.0788	415	24.3	5.8	18.1	0.4
8	400	0.1602	441	46.8	11.6	34.0	1.2
9	400	0.339	497	90.1	20.5	68.0	1.6
10	700	0.0387	681	9.0	2.2	6.6	0.2
11	700	0.0776	690	17.6	4.5	12.7	0.4
12	700	0.1603	713	35.0	8.0	26.4	0.6
13	400	0.1227	430	34.2	8.1	25.5	0.6
14	1,000	0.0841	965	13.7	3.4	9.9	0.4

DISCUSSION

The relative importance of radiation as a contributing mechanism in the transfer of heat through the gas-solid bed may be obtained from the total local conductivity and an estimate of the local conduction conductivity. The local radiation conductivity is the difference between these quantities. The temperature dependence of the ratio of the radiation and conduction conductivities then shows the relative magnitude and rate of increase with temperature of the radiation contribution.

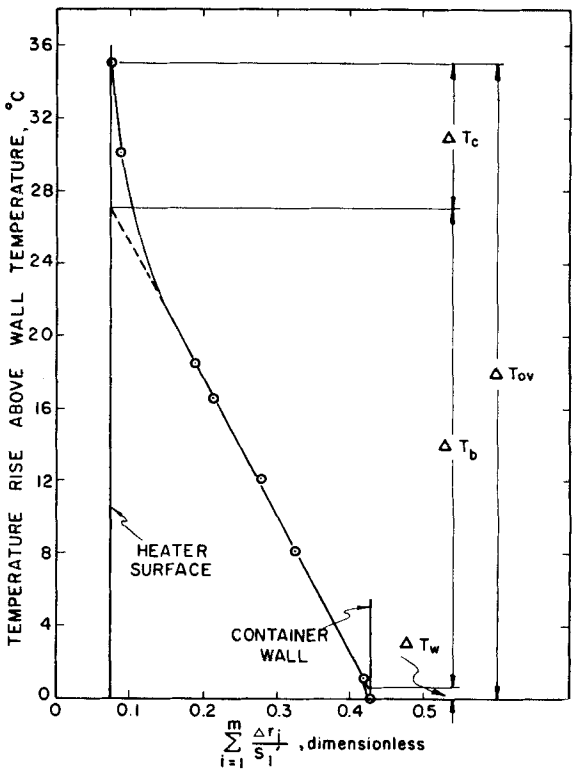

Fig. 6. Mid-plane radial temperature distribution, experiment 12.

TABLE 4. CONDUCTIVITIES AND BOUNDARY HEAT TRANSFER COEFFICIENTS WITH AVERAGE TEMPERATURES

Experiment no.	$10^5 k_{0v}$, cal./(sec.)(cm.)(°C.)	T, °C.	$10^5 k_b$, cal./(sec.)(cm.)(°C.)	T, °C.	$10^5 h_c$, cal./(sec.)(sq. cm.)(°C.)	T, °C.	$10^5 h_w$, cal./(sec.)(sq. cm.)(°C.)	T, °C
1	85	113	105	111	560	119	240	105
2	76	92	111	91	290	93	220	90
3	108	140	110	141	...	...	260	127
4	73	190	111	179	260	214	200	155
5	94	141	111	139	810	154	300	126
6	109	408	163	406	400	412	340	402
7	114	427	153	424	530	436	520	415
8	120	464	166	459	530	482	350	442
9	132	542	175	533	640	577	560	498
10	151	685	206	684	680	689	510	681
11	155	699	214	697	670	706	510	690
12	161	731	213	727	780	744	710	713
13	126	447	163	443	590	460	540	430
14	216	972	298	970	960	977	560	965

Two types of comparison of theory and experiment may be made with the estimates of the radiation and conduction contributions. In one case values of the parameter, $\rho - \tau$, may be obtained from values of the local radiation conductivity used in conjunction with Equation (8). In the other, boundary heat transfer coefficients and the radiation and conduction conductivities may be used in an equation obtained from Hamaker's work to evaluate the parameter, $\rho + \tau$.

Each of the calculations indicated above assumes that the only heat transfer mechanisms present in the experiments were conduction and radiation; that is, convection was absent, and conduction and radiation did not interact. Therefore, the suitability of the data for such use will be considered before calculations are made.

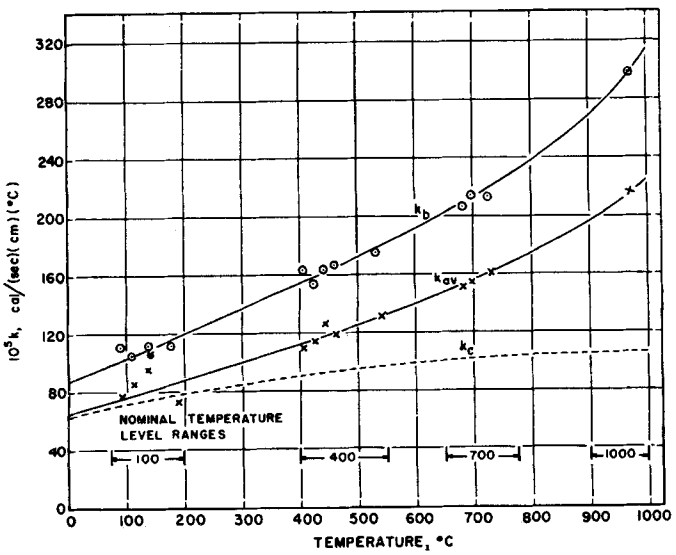

Fig. 7. Over-all and local bed thermal conductivities.

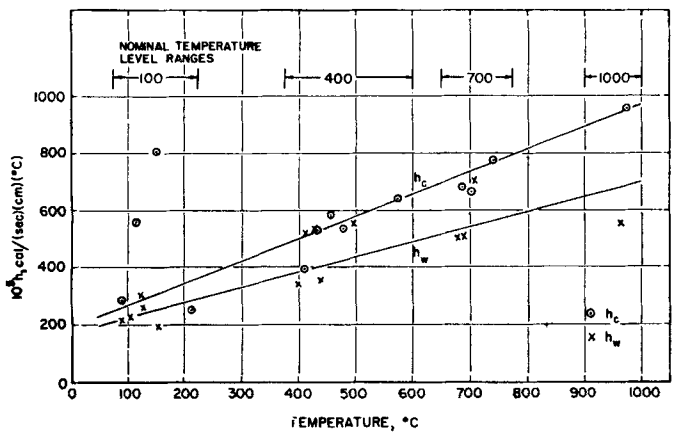

Fig. 8. Apparent boundary heat transfer coefficients.

Absence of Convection or Interaction of Radiation and Conduction

With reference to Figures 7 and 8, if one were to extrapolate the conductivities or heat transfer coefficients obtained as a function of temperature gradient at a given temperature level to zero gradient, and if this were done at a series of temperature levels, the extrapolated points would define the temperature dependence of the conductivity or heat transfer coefficient due to mechanisms other than convection, that is due to conduction and radiation alone. Further in the case of local conductivities the contributions of conduction and radiation would be additive, since Held (*7*) has shown that for sufficiently small temperature gradients the two processes take place in parallel without interaction. It was the intention in the present work to use these facts to determine whether convection or interaction of conduction and radiation was present in the experiments. Thus a departure from the zero-gradient curve would be an indication of the presence of these mechanisms. However the scatter of the data was such, particularly in the case of the boundary coefficients, that the solid curves in Figures 7 and 8, rather than being based on extrapolations to zero temperature gradient at the background temperature level, were drawn considering all of the data. Nevertheless in the case of the conductivities, temperature level, rather than temperature gradient, was the important variable. Thus effects of temperature gradient, such as convection and interaction of conduction and radiation, apparently were not present to an extent which was discernible by the method indicated, and in the ensuing calculations it was assumed that they were absent.

Ratio of Radiation to Conduction Heat Transfer

The conduction conductivity was estimated by means of the modified correlation of Schumann and Voss (*28*), which was assumed to predict k_c at any given temperature when the values of k_s and k_g corresponding to the given temperature were substituted in it. A value of 1.8 B.t.u./(hr.)(ft.)(°F.) for k_s at 1,000°C. was given by the manufacturer (*14*). It was then assumed that the temperature dependence of k_s was the same, on the basis of percentage, as that given for aluminum oxide by Jakob (*9*). The conductivity of air was taken from Glassmann and Bonilla (*5*). The results are plotted along with the experimental k_b and k_{ov} in Figure 7. It is seen that k_c is substantially lower than k_b even at low temperature but that it is in good agreement with k_{ov} at low temperature. Reasonable agreement might be expected,

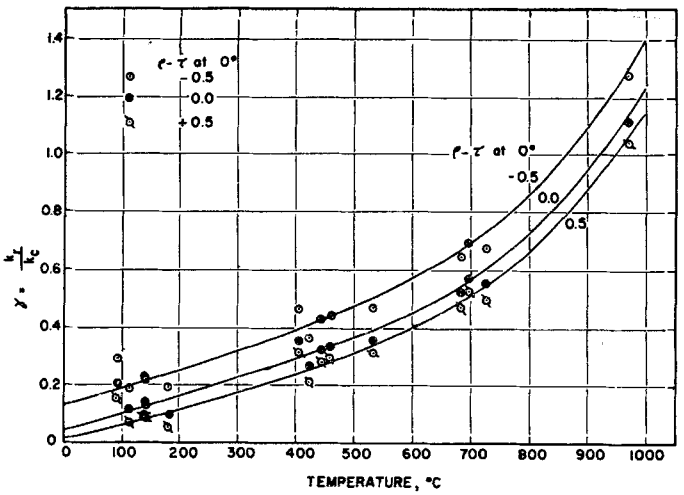

Fig. 9. Ratio of heat transfer by radiation to heat transfer by conduction.

since Schumann and Voss's correlation was based on room temperature experiments in which what has been identified here as k_{ov} was measured. Actually the agreement is better than expected and is partly fortuitous since the correlation was based on continuous distance coordinates.

In order to proceed further it was assumed that the predicted temperature dependence of k_c was valid and that, since k_b and k_{ov} exhibit similar temperature dependence, the values for k_c might be adjusted by the factor necessary to give good agreement with k_b at 0°C. In making the adjustment it was necessary to assume a value of $\rho - \tau$ at 0°C., for this quantity fixes k_r and hence k_c at 0°C. Three values of $\rho - \tau$ at 0° were assumed: -0.5, 0, $+0.5$. These values were assumed to cover the practical range of this difference. Then with $T = 273$°K. these values were inserted in Equation (8). The radius increment was assumed constant at 0.39 cm., and the average values of S_m'/S_m, 1.12, and S_m'/S_{m+1}, 0.90, in the vicinity of the linear portion of the bed radial-temperature distribution were used.

Having fixed k_c at 0°C. and adjusted k_c at all other temperatures accordingly, one obtained values of k_r by subtracting k_c from the smooth curve for k_b. The ratio, $\gamma = k_r/k_c$, is plotted in Figure 9 as a function of the average temperature of the temperature drop ΔT_b for all values of $\rho - \tau$ at 0°C. At room temperature the value of γ is about 0.1, and heat transfer by radiation is of the order of 10% of the total heat transfer. At high temperatures (1,000°C.) γ increases to about 1.2, and radiation heat transfer accounts for about 55% of the total.

Evaluation of $\rho - \tau$

From k_r and Equation (8) values of $\rho - \tau$ were obtained at all temperatures for each assumed value of $\rho - \tau$ at 0°. The results are shown in Figure 10 plotted against the average temperature of the temperature drop ΔT_b. It is seen that above 200° $\rho - \tau$ increases with temperature. This behavior would be expected at all temperatures, since for refractory materials the reflectivity increases with temperature and it would seem reasonable that the transmissivity of a packed bed would be relatively insensitive to temperature. The initial decrease of $\rho - \tau$ with temperature in two of the curves is unreasonable on this basis and may be due to the shape of the correlation used to predict k_c in the low temperature range. The curve used for k_b is concave upward, while those for k_c are concave downward. This fact is emphasized at low temperatures and large values of $\rho - \tau$ at 0° where the difference, k_r, is smallest. No significance is attached to the slight decrease in $\rho - \tau$ at 1,000° since whether the curves increase monotonically or exhibit maxima at about 900° depends on how one draws the relation between k_b and temperature in Figure 7 in the vicinity of 800 to 1,000° where there is but one experimental point. A sharper maximum is obtained if the curve for k_b rises more sharply.

It may be noted that all curves converge approximately to a value of 0.4 at 1,000°. Convergence might be expected, since γ is greatest here and slight changes in the assumed value of k_c have little effect on the resulting value of k_r and the value of $\rho - \tau$ calculated from k_r.

Even though the necessary assumptions make these calculations only approximate, it is interesting to see what values of p and T are consistent with them. Extrapolating values of R for aluminum oxide taken from Jakob (*9*) one finds that $R = 0.82$ at 1,000°C. When one uses this value and $\rho - \tau = 0.4$ at 1,000°, it is found on substituting in Equation (12) that this equation can be satisfied only by $0.7 < p < 1.0$ and $0 < T < 0.2$. The values for T are somewhat lower than estimates which one might be tempted to use. Thus one might improperly identify T with an estimate of the geometrical fraction free area, $f^{2/3}$, which in the case of these experiments would make $T = 0.52$.

More accurate and more direct estimation of radiation constants may be obtained by measurements either of the reflectivity of an exterior surface of an isothermal bed as a function of bed thickness and temperature or of transmission through such a bed. Measurements of the latter type have been made on porous and fibrous insulation by Verschoor and Greebler (*25*) and Larkin and Churchill (*11*). Equations useful for these purposes have been derived by Hamaker (*6*) for the flat-plate geometry. For other geometries the equations may be derived by solving Equations (1) and (2) simultaneously with $W_m = W_0$, the radiant emission corresponding to the constant temperature T_0 throughout the bed. Once accurate estimates of radiation constants are obtained, it would then be possible in heat transfer experiments to obtain values of k_c at high temperatures. This constant has been measured at low temperatures only where virtually all of the heat is transferred by conduction.

Evaluation of $\rho + \tau$

Hamaker (*6*) solved the equations for simultaneous conduction and radiation for the flat-plate geometry expressed in continuous distance coordinates. The corresponding solution from the present theory has not been found. The relation obtained by Hamaker for the apparent boundary temperature discontinuity is

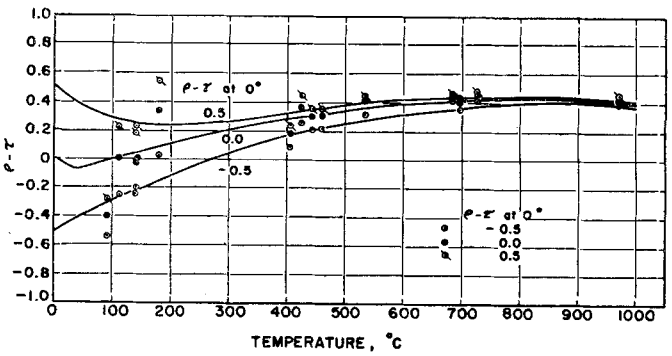

Fig. 10. Values of $\rho - \tau$ derived from data.

presented here rearranged and expressed as a heat transfer coefficient. Hamaker's absorption coefficient a has been replaced by $a = \alpha/\Delta r$:

$$h_w = \frac{8\sigma T^3}{S_w}\left(\frac{1+\gamma}{\gamma}\right)^2 \cdot \left[\sqrt{\frac{\alpha k_c}{8\sigma T^3\,\Delta r}\left(\frac{\gamma}{1+\gamma}\right)} + \frac{1-\rho_w}{1+\rho_w}\right] \tag{15}$$

All quantities in this relation may be obtained from experiments of the type described in this paper except the bed absorptivity, the conduction conductivity, and the reflectivity of the bounding surface. If estimates of k_c and ρ_w are available, then $\alpha = 1 - (\rho + \tau)$, and in turn $\rho + \tau$ may be calculated. It must be assumed that the equation applies when the boundary temperature discontinuities and hence the boundary heat transfer coefficients are obtained from plots of temperature vs. $\sum_{i=1}^{m} (\Delta r_i/S_i')$. Such calculations were made for both bounding surfaces with experimental values for h_w, S_w, T and Δr, values of k_c and γ derived from the data, and values for ρ_w taken from McAdams (*13*). For all values of $\rho - \tau$ at 0° (which determined k_c and γ) $\rho + \tau$ was found to decrease with temperature, whereas it should increase with temperature. Moreover agreement of values obtained at the two surfaces was poor, and values at the container surface were in some cases negative. These results indicate that the phenomena causing boundary temperature discontinuities may not primarily involve interaction of radiation and conduction. A further calculation indicated that conduction alone may cause the discontinuities.

The boundary coefficients increased by a factor of 3 to 4 over the temperature range of 100° to 975°. The conductivity of air increases by a factor of 2.5 over the same temperature range, and if one sets

$$h_w = \frac{k_{air}}{\Delta r_{air}} \tag{16}$$

it is found that effectively an air film existed of 0.2- to 0.3-mm. thickness at the heater and 0.3- to 0.4-mm. thickness at the container surface. No significance is necessarily attached to the difference in thicknesses at the two boundaries. Thus it is suggested that the boundary heat transfer mechanism primarily involved conduction across an air film. A similar conclusion was drawn by Pollack (*18*).

CONCLUSIONS

1. The theory of Hamaker was generalized to permit consideration of spherical and cylindrical as well as planar geometries. The generalization was expressed in terms of finite differences, a form appropriate for particulate systems. The conductivity of the radiation model was derived.

2. Unidirectional heat transfer rates and the corresponding temperature distributions were measured in a fixed bed of ceramic particles and air at atmospheric pressure over the temperature range 100° to 1,000°C. Conductivities and boundary heat transfer coefficients increased with temperature level. No effect of temperature gradient was discernible.

3. With the use of the theoretical expression for the radiation conductivity and independent estimates of the conduction conductivity, values of γ, the ratio of radiation to conduction heat transfer rates in the bed, and $\rho - \tau$, the difference between the reflectivity and the transmissivity of a layer of particles one average particle spacing thick, were derived from the data. Values of γ increased from about 0.1 at 100°C. to 1.2 at 1,000°C. The value of $\rho - \tau$ at 1,000°C. was 0.4.

4. Boundary temperature discontinuities could better be ascribed to imperfect thermal contact and not to interaction of conduction and radiation. Local conductivities in the bed proper exceeded over-all conductivities by 40% at all temperatures.

5. It was suggested that the estimates of $\rho - \tau$ deducted here from heat transfer experiments should be refined by means of optical measurement of the effective radiation characteristics of isothermal beds and that then it would be possible in subsequent heat transfer experiments to characterize conduction at high temperatures.

ACKNOWLEDGMENT

This work was supported by generous financial aid in the form of a fellowship grant from the Pittsburgh Consolidation Coal Company. The authors are indebted to W. L. Dennison of the Princeton University Infirmary for X-ray pictures of Calrod heaters, to the Radio Corporation of America for thermocouple fabrication, and to the Johns-Manville Corporation for the supply of insulation.

NOTATION

Dimensional Units

L = length
M = mass
H = quantity of heat
θ = time
T = temperature

Letter Symbols

a = absorption coefficient (L^{-1})
A = absorptivity of surface of gray ceramic particle (dimensionless)
D_p = particle diameter (L)
f = fraction void (dimensionless)
h_c = heat transfer coefficient at Calrod heater surface ($H/L^2\theta T$)
h_w = heat transfer coefficient at the container wall, or at any boundary ($H/L^2\theta T$)
i = surface i
i^+ = convex side of surface i
i^- = concave side of surface i
I_m = radiance energy of reference area, S_m, of convex side of surface m($H/\theta L$ for cylinders, H/θ for spheres)
I'_m = quantity defined by Equation (4) (units same as for I_m)
J_m = radiance energy of reference area, S_m, of concave surface of surface m (units same as for I_m)
J'_m = quantity defined by Equation (5) (units same as for I_m)
k_{air} = thermal conductivity of air ($H/L\theta T$)
k_b = total local thermal conductivity of particle bed far from bounding surfaces ($H/\theta LT$)
k_c = average local thermal conductivity due to conduction in particle bed ($H/\theta LT$)
k_{c_m} = thermal conductivity due to conduction at position m in particle bed ($H/\theta LT$)
k_g = thermal conductivity of gas phase ($H/\theta LT$)
k_{ov} = total thermal conductivity of particle bed including effect of bounding surfaces ($H/\theta LT$)
k_r = average local thermal conductivity due to radiation in a particle bed ($H/\theta LT$)
k_{r_m} = k_r at position m ($H/\theta LT$)
k_s = thermal conductivity of solid phase ($H/\theta LT$): see m, m^+, m^-; i, i^+, i^-
N = number of concentric surfaces representing particle bed(dimensionless)
p = fraction of radiation incident on a particle which is scattered backward (dimensionless)
Q = heat transfer rate through reference area in a direction normal to S_m (units same as for I_m)
r_m = radial position of $m-th$ surface (L)
Δr = average particle spacing (L)
Δr_{air} = effective thickness of air film (L)
Δr_m = Δr at position m(L)
R = reflectivity of surface of gray ceramic particle (dimensionless)
S_m = reference area of surface m: area per unit axial length for concentric cylinders (L), area per sphere for spheres (L^2)
S_m' = area appropriate for conduction heat transfer normal to and through the region bounded by S_m and S_{m+1} (units same as for S_m)
S_w = reference area of a bounding surface (units same as for S_m)
T = absolute temperature (T); fraction of energy of rays incident on a layer of particles which is transmitted through layer apart from reflection (dimensionless)

T_m = absolute temperature of surface m (T)
ΔT_b = temperature drop across bed based on linear portion of distribution in bed (T)
ΔT_c = temperature discontinuity at heater surface (T)
ΔT_{ov} = over-all temperature drop across bed (T)
ΔT_w = temperature discontinuity at container wall (T)
W_m = radiant energy emitted by reference area S_m per unit time (units same as for I_m)

Greek Letters

α = average effective absorptivity of gray surface of layer of particles one average particle spacing thick (dimensionless)
α_m = effective absorptivity of gray surface m (dimensionless)
γ = ratio of heat transfer by radiation to heat transfer by conduction (dimensionless)
ρ = average effective reflectivity of gray surface of layer of particles one average particle spacing thick (dimensionless)
ρ_m = effective reflectivity of gray surface m (dimensionless)
ρ_w = reflectivity of an opaque bounding surface (dimensionless)
σ = Stefan-Boltzmann constant, 1.378×10^{-12} cal./(sec.)(sq. cm.)(°K.)^4
τ = average effective transmissivity of layer of particles one average particle spacing thick (dimensionless)

LITERATURE CITED

1. Bosworth, R. C. L., "Heat Transfer Phenomena," John Wiley, New York (1952).
2. Campbell, J. M., and R. L. Huntington, *Petrol. Refiner*, **31**, 123 (1952).
3. Christiansen, C., *Ann. Physik. Chem.*, **19**, 267 (1883).
4. Damköhler, G., "Der Chemie-Ingenieur," Eucken-Jakob, Vol. III, Part 1, p. 445, Akademische Verlagsgesellschaft M.B.H., Leipzig, Germany (1937).
5. Glassmann, Irvin, and C. F. Bonilla, *Chem. Eng. Progr. Symposium Ser., No. 5*, **49**, 153 (1953).
6. Hamaker, H. C., *Philips Research Repts.*, **2**, 55, 103, 112, 420 (1947).
7. Held, E. F. M. van der, *Appl. Sci. Res.*, **A3**, 237 (1953); **A4**, 77 (1954).
8. Hill, F. B., Ph.D. thesis, Princeton Univ., Princeton, New Jersey (1958).
9. Jakob, Max, "Heat Transfer," John Wiley, New York (1949).
10. Kistler, S. S., *J. Phys. Chem.*, **39**, 79 (1935).
11. Larkin, B. K., and S. W. Churchill, *A.I.Ch.E. Journal*, **5**, No. 4, 467 (1959).
12. Lucks, C. F., O. L. Linebrink, and K. L. Johnson, *Trans. Am. Foundrymen's Assoc.*, **55**, 62 (1947); **56**, 363 (1948).
13. McAdams, W. H., "Heat Transmission," 3 ed., McGraw-Hill, New York (1954).
14. Norton Co., personal communication.
15. Norton, F. H., and W. D. Kingery, "The Measurement of Thermal Conductivity of Refractory Materials," Quarterly Progress Report for the Period Ending April 1, 1955, NYO-6449, Mass. Inst. Technol., Cambridge.
16. Nusselt, W., *Z. bayer. Revisions.-ver.*, **17**, No. 13 and 14 (1913).
17. Pirani, M., and von Wangenheim, *Z. tech. Physik.*, **10**, 413 (1929).
18. Pollack, J. A., Sc.D. thesis, Mass. Inst. Technol., Cambridge (1948).
19. Prins, J. A., J. Schenk, and A. J. G. L. Schram, *Physica*, **16**, 379 (1950).
20. Russell, H. W., *J. Am. Ceram. Soc.*, **18**, 1 (1935).
21. Saunders, O. A., *Proc. Phys. Soc. (London)*, **41**, 569 (1929).
22. Schumann, T. E. W., and V. Voss, *Fuel*, **13**, 249 (1934).
23. Smith, W. O., *Physics*, **1**, 18 (1931).
24. Van Rinsum, W., *Beilage zu Forsch. Gebiete Ingenieurw.*, **228** (1920).
25. Verschoor, J. D., and P. Greebler, *Trans. Am. Soc. Mech. Engrs.*, **74**, 961 (1952).
26. Waddams, A. L., *Chem. & Ind. (London)*, p. 206 (1944).
27. Weininger, J. L., and W. G. Schneider, *Ind. Eng. Chem.*, **43**, 1229 (1951).
28. Wilhelm, R. H., W. L. Johnson, R. Wynkoop, and D. W. Collier, *Chem. Eng. Progr.*, **44**, 105 (1948).

Manuscript received November 5, 1958; revision received April 29, 1959; paper accepted May 5, 1959. Paper presented at A.I.Ch.E.-A.S.M.E. 1958 Heat Transfer Conference.

The Vapor-phase Catalytic Hydration of Ethylene Oxide to Glycols

A. B. METZNER and J. E. EHRREICH

University of Delaware, Newark, Delaware

The vapor-phase reaction between ethylene oxide and water to form glycols has been carried out under a wide range of conditions with particles of polystyrene-sulfonic acid ion exchange resins used as catalysts. The rates observed appeared to be directly proportional to the product of the partial pressure of ethylene oxide and the amount of water sorbed by the resin. By use of the Brunauer, Emmett, and Teller equation to describe the amount of water sorbed by the resin, the experimental data were correlated over a sixty-fold range of reaction rates with a mean deviation of 15%.

To obtain data of value in elucidating reaction mechanisms, the reactor was usually run under "differential" conditions, that is low conversions. However in a few runs conversions of as high as 54% were obtained for a contact time of 0.02 sec. The ratio of ethylene glycol to higher glycols (selectivity) obtained varied between 73 and 99% but was usually above 80% under conditions of high conversion. However it could also be reduced forcibly to produce higher glycols as the major product, if desired.

The growing demand for ethyleneglycol has stimulated a great deal of research. Until recently all the ethylene oxide hydration studies were concentrated on understanding the homogeneous reaction, primarily the sulfuric-acid catalyzed reaction (*2, 5, 11, 12, 14*) between water and dissolved ethylene oxide. Of the heterogeneous solid catalyzed reactions, the more interesting ones appear to be those involving a strong hydrogen ion exchange resin as the catalyst. Othmer and Thakar (*12*) studied the use of batch and fluidized beds for the liquid-solid heterogeneous system. Reed, Wenzel, and O'Hara (*15*) published data on a continuous packed-bed reactor for the vapor-solid and vapor-

J. E. Ehrreich is with the Dewey and Almy Chemicals Company, Cambridge, Massachusetts.